ACS Macro Letters

Letter

pubs.acs.org/macroletters

Semiquantitative Structural Analysis of Highly Anisotropic Cellulose Nanocolloids

Kojiro Uetani and Hiroyuki Yano*

Division of Creative Research and Development of Humanosphere, Research Institute for Sustainable Humanosphere, Kyoto University, Gokasho, Uji, Kyoto 611-0011, Japan

Supporting Information

ABSTRACT: We report a method for the semiquantitative structural analysis of highly anisotropic nanocolloids by means of their "coffee rings", which were readily formed via the evaporation of droplets of the cellulose nanocolloidal suspensions. The widths of the coffee rings reflected the effective aspect ratios and the conformation of the colloids in water, owing to the excluded volume effect. The theory developed here succeeded in estimating the relative length of the cellulose nanofibrils, which were obtained from Japanese cedar pulp using a grinder, as 11.33 μm. The coffee rings allow the comprehensive structures of colloids to be semiquantitatively revealed and also allow the length or size of colloids in different systems to be compared.

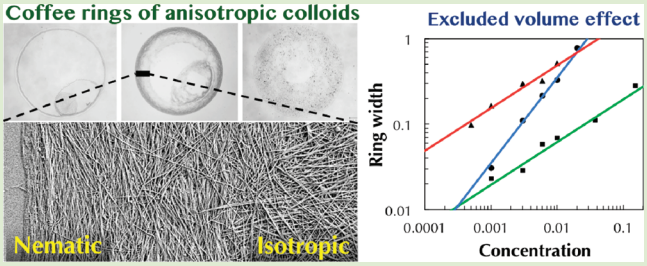

Cellulose nanoparticles (CNPs), including nanofibrils and nanowhiskers, have been extensively promoted for use in various bulk materials; these materials are most often obtained from abundant green resources.[1−5] The nanoscale effects of CNPs have been investigated in homogeneous materials, and more fundamental properties arising from their dimensions have been characterized using chemical decomposition,[6] rheology,[7,8] dynamic light scattering,[9] and small-angle X-ray scattering.[10] However, despite this great interest, there is still no versatile method for the estimation—or even comparison—of the "length" of these highly anisotropic, often polydisperse nanocolloids; only the fibril diameters or the size of much shorter, individual whiskers or rods have been measured, via direct observation.[6−9,11] The length of anisotropic colloids including chitin, collagen, fibroins, and other bionanofibers, which are often obtained by the miniaturization of raw materials, is of importance as the most fundamental parameter, not only for material design but also for the analysis of natural products. There is therefore a need for a standard method for the structure analysis of colloids.

Plants control cellulose microfibrils to grow precisely patterned cell walls for specific purposes. While it is desirable to control these highly anisotropic nanocolloids to achieve 2D or 3D patterning and create sophisticated materials such as cell walls, there is little knowledge regarding the transportation and structuration behavior of these colloids in solution.

In this study, we analyzed the "coffee rings" of three kinds of CNPs to investigate their transportation behaviors and found that the concentration dependence of the resulting ring widths reflected the effects of the aspect ratios and conformations of the colloids in water. A coffee ring (a ring-shaped deposition of colloidal particles) is readily observed when a coffee drop dries on a table. This occurs largely because of the pinning of the contact line of the droplet by the deposited particles, and the outward capillary flow to the contact line generated by the regional change in the evaporation flux.[12] This phenomenon, known as the coffee ring effect, is applied directly to create transparent conductive coatings,[13] and ordered assemblies.[14,15] The coffee ring deposition process is similar to the flow-induced enrichment process for colloidal particles. We focused on the differences in the excluded volume effects induced by the anisotropy during enrichment, which produced the different packing fractions in the rings.

We produced three kinds of CNPs: cotton nanowhiskers (CNWs), tunicin nanowhiskers (TNWs), and sugi nanofibrils (SNFs) (Figure 1a−c), from cotton fibers, tunicate of ascidian, and Japanese cedar (sugi), respectively (see the Supporting Information). The size distributions of ∼200 whiskers, individually measured using a TEM, showed a rough power-law tendency, with logarithmic normal distributions (Figure 1d). The median diameter of the CNWs, d_C, was 28.03 nm, and that of the TNWs, d_T, was 30.57 nm. The median length of the CNWs, L_C, was 279.74 nm, and that of the TNWs, L_T, was 2312.62 nm. Both types of whiskers showed pronounced polydispersity, but here we discuss the effect of the aspect ratios α (L/d) of these whiskers, using their median sizes as representative values. The TNWs were 8.3 times longer than the CNWs. On the other hand, the SNFs, which were fibrillated by the grinder,[9] were observed to be long, bent, or coiled and to have random bundles and branches, whereas the whiskers were observed to be rod-like particles. The median diameter of the

Received: March 7, 2012
Accepted: May 1, 2012
Published: May 8, 2012

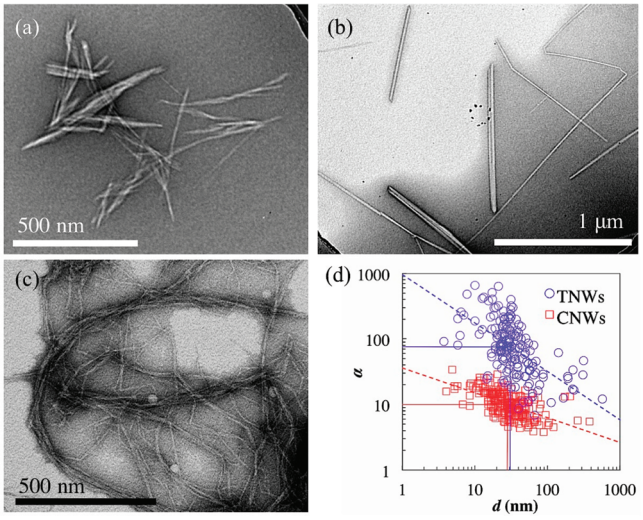

Figure 1. Transmittance electron micrographs of CNWs (a), TNWs (b), and SNFs (c). The size distributions of the whiskers [the diameter (d) vs the aspect ratio (α)] show a rough power law tendency, with logarithmic normal distributions (d). The dashed lines represent the regression lines for the power law, and the solid lines indicate the median values.

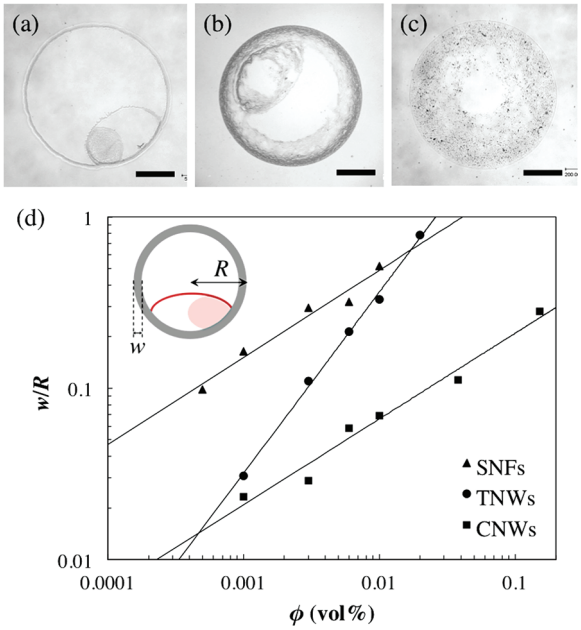

Figure 2. Optical micrographs of (a) CNW, (b) TNW, and (c) SNF stains left on the substrate after the evaporation of a 1 μL droplet of a 0.01 vol % suspension. Note 500 μm scale bars in lower right corners. (d) The width of the ring (w) at depinning normalized by the droplet radius ($R \approx 1$ mm) vs the concentration (ϕ). A best fit to a power law gave an exponent of 0.51 ± 0.01 for the SNFs, 0.50 ± 0.01 for the CNWs, and 1.06 ± 0.01 for the TNWs. The inset shows the schematic illustration of a typical CNW coffee ring, with twice depinning.

SNFs was 19.23 nm, and the arithmetic average diameter was 32.91 nm. Here, our objective was to reveal the conformational structure and size of the SNFs in solution, using a comparison with the whiskers to estimate the length of the SNFs, L_S.

The equilibrium zeta potential[9] values under the conditions used for the coffee ring formation were −61 mV for the CNWs, −64 mV for the TNWs, and −57 mV for the SNFs. The thickness of the electric double layer (the Debye screening length, κ^{-1}) is non-negligible for colloidal systems with particle concentrations greater than or equal to that of a semidilute solution.[16,17] On the other hand, the suspension droplets containing just 0.1 mM salt (e.g., KCl), to define κ^{-1} clearly, formed crystallized salt, which precipitated on the coffee rings as the droplets evaporated, and the colloidal coffee rings became invisible or partially did not form. We therefore removed the salt ions from the suspensions using thorough filtration and dilution with Milli-Q water; we then determined the κ^{-1} for the CNPs from the residual electrolyte concentration, which was determined using the electric conductivity measured for each suspension[16] (see the Supporting Information). The suspensions of both types of whiskers, which were purified from an H_2SO_4 solution for acid hydrolysis, were considered to predominantly contain H_3O^+ and SO_4^{2-} ions. The κ^{-1} values were then determined to be 36.55 nm for the CNWs and 25.10 nm for the TNWs. The SNF suspension, which was purified using the Wise method,[18] was thought to contain mostly monovalent Na^+ and COO^- ions. The κ^{-1} for the SNFs was then determined as 28.04 nm. The effective diameter of the whiskers was defined as $d_{eff} = d + 2\kappa^{-1}$ and the effective length as $L_{eff} = L + 2\kappa^{-1}$, so the effective aspect ratios α_{eff} became smaller than α during the ring formation.

We evaporated the CNP suspensions on cover glasses (see the Supporting Information) and observed that each colloid in the droplets was transported near the contact lines to form the deposit, in accordance with the coffee ring effect (Figure 2a–c). An obvious difference was detected in the initial concentration ϕ versus the ring width w at the first depinning (normalized by the droplet radius R) for the CNPs (Figure 2d). In more dilute conditions, the TNWs showed a w/R value similar to that shown by the CNWs; this became closer to the value shown by the SNFs as ϕ increased. The subequal exponents (of approximately 0.5) of the CNWs and the SNFs indicated some similarity between them.

The contact angles θ_c and their decrease under evaporation (normalized by t_{total}, the lifetime of the droplets) were measured using the half-angle method, which holds for the relation $h/R = \tan(\theta_c/2)$, where h is the central height of a spherical droplet (Figure 3a). The CNP suspensions showed similar θ_c for ϕ values from 0.001 to ∼0.1 vol % (inset in Figure 3a). It was striking that the SNF droplets experienced almost no depinning events during evaporation, whereas those of the CNWs and the TNWs typically experienced single or double depinning events at t_{d1} or t_{d2} at the end of the evaporation process, respectively, regardless of ϕ. This remarkable long pinning, which has rarely been reported for spherical colloids, is thought to be the cause of the hydrophilicity and in particular the continuity of the high-anisotropy CNPs.

The mass of the evaporating 1 μL droplets was reduced linearly as a function of t (Figure 3b). The effective total drying time, t_f, determined by a linear extrapolation of the mass reduction,[19] was very close to t_{d1} or t_{total}, and t_f got closer to t_{total} as the number of depinning events decreased. The evaporation flux dM/dt showed no significant difference between the samples, at various ϕ (inset in Figure 3b). As the droplets evaporated, the ion concentrations in the suspensions increased. However, even when the ionic strength became 10 times stronger as the 1 mg droplet evaporated to 0.1 mg, the colloidal stability (zeta potentials) changed little in our case, because the initial ion concentrations were still quite low (e.g.,

dx.doi.org/10.1021/mz300109v | ACS Macro Lett. 2012, 1, 651–655

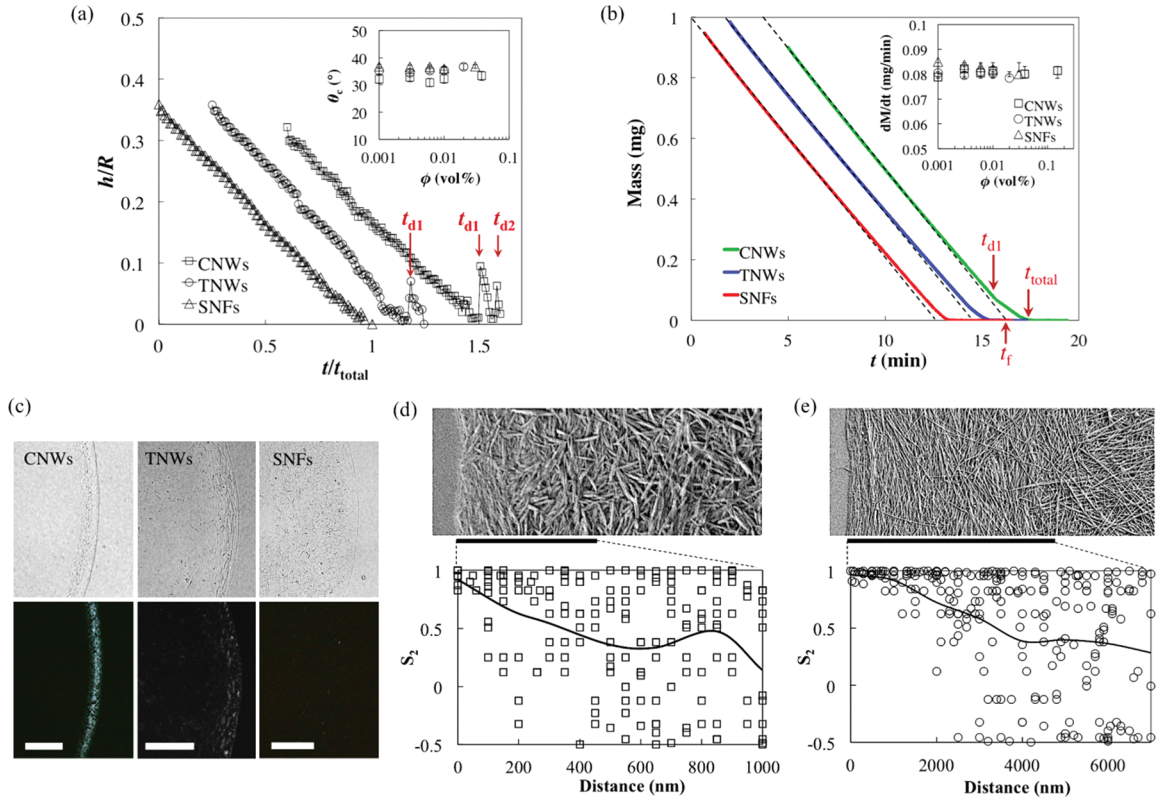

Figure 3. Contact angles (h/R = tan (θ_c/2)) of evaporating droplets vs time t, normalized by the total evaporation time t_{total} (a). Here, the TNW data set has been shifted by +0.3, and that of the CNWs has been shifted by +0.6, to allow a better view of the data. The arrows indicate the first and second depinning times, t_{d1} and t_{d2}, respectively. The inset shows the static contact angle θ_c vs the CNP concentration. The mass reduction of the evaporating droplets as a function of t (b). Both data sets were shifted 2 min from each other to better illustrate the data. The early time data are suppressed, because they contain transients due to the settling time. The arrows indicate t_{d1}, t_{total}, and the extrapolated drying time, labeled t_f. The inset shows the rate of mass loss by evaporation, dM/dt, vs the CNP concentration. Polarized micrographs of CNPs (c) with 200-μm scale bars. Field emission scanning electron micrographs of CNW coffee ring edges (d) and TNWs (e) revealed the orientational order parameter S_2 as a function of distance from the contact lines to the center of the rod-like whiskers. The solid lines connect the average S_2 values on each 100 nm (d) and 1 μm (e), $\overline{S}$.

2.32×10^{-5} M for CNWs with a zeta potential of −61 mV might have become concentrated to 2×10^{-4} M, with −55 mV). The 10-times-concentrated whisker droplets then started depinning (Figure 3b), and the coffee ring formation was finished. We assumed that the low ionic strength in the initial suspensions meant that we could ignore the slight change in the colloidal stability that occurred during the coffee ring formation.

The CNW and TNW rings showed birefringence, whereas those made up of SNFs did not (Figure 3c). The TNW rings near the contact line showed stronger birefringence, while the inner rings showed weaker effects. The FE-SEM images clarified the isotropic−nematic transition of the whiskers[20,21] at the ring edges (Figure 3d,e), which occurred independent of ϕ. The CNWs with an α_{eff} of ∼3.5 formed rougher nematic regions than the TNWs with α_{eff} of ∼29.3; the SNFs showed no structuration in the rings, because of the arbitrarily curved structure. We investigated the orientational order parameter $S_2(\cos\theta_r) = \langle 1.5\cos^2\theta_r - 0.5\rangle$, where θ_r is the whisker's angle relative to the contact line, as a function of distance. For both whisker types, close to the contact lines the mean S_2 at regular intervals $\overline{S}$ showed a value of almost 1 and gradually decreased to approach 0. Assuming that the transition point was at $\overline{S}$ = 0.5, the widths of the nematic region were almost equal to the median lengths of each whisker. Since the colloidal system in the droplets was stabilized predominantly by the repulsion due to the surface charge on the CNPs, it was concluded that this isotropic−nematic transition derived from the occurrence of enrichment during the ring formation, in accordance with Onsager's covolume theory.[22] The orientation of the highly anisotropic particles at the ring perimeter was dominated not only by the flow velocity[23] but also by the minimization of the free energy (maximization of entropy) of the system during the enrichment process.

Based on the preconditions investigated so far, we analyzed the concentration dependence of the ring widths (w/R vs ϕ) theoretically, to characterize the anisotropy and conformations of the CNPs (Figure 2d). Deegan estimated w at the first depinning for spherical colloids in terms of ϕ, as follows:[19]

$$\frac{w}{R} = \sqrt{\frac{\phi}{4p}}\left[1 - \left(1 - \frac{t}{t_f}\right)^{3/4}\right]^{2/3} \quad (1)$$

which was given by the equality of the ring volume—assuming its cross section as a right-angled triangle (Figure 4a)—and the volume of the deposited particles with a mean packing fraction p at time t, from an initial droplet with a volume fraction ϕ. Equation 1 is applicable when $t \ll t_f$, when the flow velocity of the particle is slow and nearly constant.[23] However, our experiments showed that $t_{d1}/t_f \approx t_{d1}/t_{total} \approx 1$ (Figure 3a,b), so the time term in eq 1 was negligible (set to 1). We then applied

dx.doi.org/10.1021/mz300109v | ACS Macro Lett. 2012, 1, 651−655

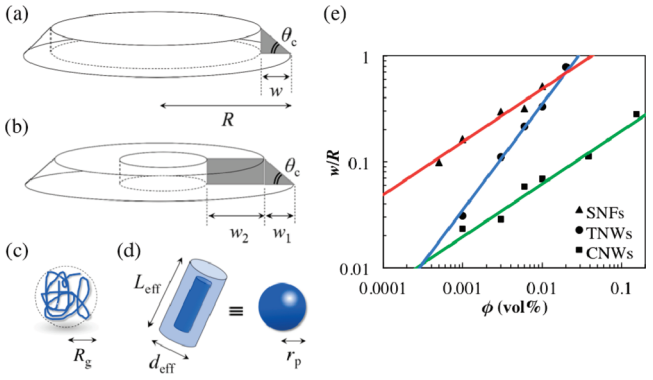

Figure 4. Explanatory diagrams of the triangular cross-section model for eq 1 (a) and the trapezoidal cross-section model for eq 2 (b), for coffee rings after evaporation. An SNF unit was assumed to be a pseudosphere with a radius R_g (c). The radius r_p of a sphere having the same volume as the effective volume of the CNWs, which should form a ring with equal w/R (green line in Figure 4e), was calculated for the estimation of R_g (d). The approximations developed in this letter fit well to each data set (e). The green and red lines were theoretically determined using eq 1, for the CNWs and SNFs, respectively. The blue line was determined using eq 2, for the TNWs.

the prefactor in eq 1 with $p = 0.656$ and obtained a good fit to the CNW data (the green line in Figure 4e). The CNWs with α_{eff} of ~3.5 were found to form coffee rings with a large p of 0.656, which was equal to that for spheres.[19]

Assuming the TNWs with high cellulose crystallinity[10] to be semirigid cylinders in water, the difference between the TNWs and the CNWs was only α_{eff}. The longer, rod-like particles had larger excluded volumes,[11] which resulted in the smaller p in the isotropic phase. The TNWs also showed an isotropic−nematic transition under the concentration gradient (Figure 3e). We here hypothesized that it would be possible to separate the TNW ring into two regions with different p. The nematic region with a large p was approximated using a triangular cross-section, using eq 1, whereas the isotropic region with a smaller p value was approximated as a thin film, because $h \ll R$. We therefore developed a novel model with a trapezoidal cross section joining the two TNW sections (Figure 4b) and obtained eq 2 in a similar manner to eq 1 (see the Supporting Information).

$$\frac{w}{R} = \frac{R\phi}{4p}\left[1 - \left(1 - \frac{t}{t_f}\right)^{3/4}\right]^{4/3} \quad (2)$$

with the approximation $w_2 \approx w$, because the width of the nematic region w_1 was negligibly small compared with w. The time term was retained here only for completeness. Equation 2 fitted well to the TNW data, with $p = 7.14 \times 10^{-3}$ (the blue line in Figure 4e). The p value for the TNWs was ~92 times smaller than the value for the CNWs. Here, the excluded volume of the TNWs, expressed as $2dL^2|\sin\Theta|$, where Θ is the angle between the rod-like particles,[17] was ~75 times larger than that of the CNWs, including their d and L, but not the thickness of κ^{-1}. The proportion of p indicated by the coffee rings was considered to be consistent with that of the theoretical excluded volume, even taking into account the polydispersity of the colloids. The coffee ring method was demonstrated to be appropriate for the semiquantitative determination of α for the particles.

SNFs with a random-coil structure in water (Figure 1c) experience intrafibril and interfibril interactions, both of which arise from the excluded volume effect. We noticed that the exponent of logarithmic w/R versus ϕ reflected p, so the similarity between the CNWs and the SNFs was considered to be their large packing fraction. The SNF units were thought to have a shape without a high α_{eff}—which the TNWs had—with a spherical form, or a steric structure with a small α_{eff}, or the excluded volume itself, like CNWs. We then assumed a pseudosphere containing a coiled SNF unit, with a radius R_g (Figure 4c). R_g also incorporated κ^{-1}, for the SNFs. We applied eq 1 to the SNF data and obtained a good fit, with an apparent packing fraction of $p_{app} = 95$ (the red line in Figure 4e). We knew that $p \leq 1$ in principle, and $p = 0.656$ in eq 1 fitted well for the small α_{eff} case described above. We also assumed that the pseudosphere sustained the radius in the flow direction during drying, because of the intrafibril and interfibril excluded volume effects. The difference between p and p_{app} was therefore considered to represent the volume fraction of the SNFs accounted for in the pseudosphere ϕ_f, so $\phi_f = p/p_{app} = 6.905 \times 10^{-3}$. Interestingly, this ϕ_f value, converted to 1.08 wt % using the density of cellulose (1.57 g cm^{-3}), corresponds to the critical concentration at which the degree of fibrillation of sugi pulps starts to decrease.[5] This fact indicated that the colloids started to aggregate when the total excluded volume exceeded the volume of the whole system.

Second, the w/R for the SNFs was 7.89 times larger than that of the CNWs, with the same p value of 0.656 for the CNWs and the SNF pseudospheres, as in eq 1 (red and green line in Figure 4e). This meant that R_g was 7.89 times larger than the radius r_p of a sphere with a volume equal to the effective volume of the CNWs (Figure 4d). We knew that the sphere with the same volume as the effective volume of the CNWs should form a ring with equal w/R (green line in Figure 4e). We then obtained a value of R_g = 693.22 nm (see the Supporting Information), and L_S was finally given by

$$L_S = \frac{V_g\phi_f}{\pi(d/2)^2} \quad (3)$$

where $V_g = (4/3)\pi R_g^3$, and d is the characteristic diameter of the objective. Under our conditions, L_S was tentatively estimated as 11.33 μm, with d = 32.91 nm (α = 344).

In conclusion, we revealed that the SNF units were coiled in a steric structure with a small α_{eff} and with the same volume as a sphere of radius 693.22 nm, with 1.08 wt %; the length was estimated as 11.33 μm. This coffee ring method allows semiquantitative volume information (i.e., $V_g\phi_f$) to be determined, owing to the excluded volume of particles; this permits a semiquantitative estimation to be made of the length of highly anisotropic colloids, as long as κ^{-1} is determined for the colloids in question. This method also allows the effective size and the conformational structure of colloids in different systems to be compared. The length of specific particles or their distribution in a single system is difficult to measure, unless they are separated chromatographically. Unlike in monodisperse systems, the rigorous quantitative determination of "length" is more difficult in polydisperse systems; this is particularly true for natural nanofibrils, which often have random bundles and branches (Figure 1c). The average volume of the units and the conformation of the colloids, which can be extracted from the behavior of whole system, become important. Since the coffee ring formation is readily and

dx.doi.org/10.1021/mz300109v | ACS Macro Lett. 2012, 1, 651−655

broadly applicable for many kinds of colloids, we believe that this coffee ring technique is a good conceptual approach for the comprehensive structural analysis of highly anisotropic colloids.

■ ASSOCIATED CONTENT

Supporting Information

Procedures and theoretical details. This material is available free of charge via the Internet at http://pubs.acs.org.

■ AUTHOR INFORMATION

Corresponding Author

*Fax: +81 774 38 3658. Tel.: +81 774 38 3669. E-mail: yano@rish.kyoto-u.ac.jp.

Notes

The authors declare no competing financial interest.

■ ACKNOWLEDGMENTS

This research was supported by a Grant-in-Aid for Scientific Research (Grant 10J04452) from the Japan Society for the Promotion of Science (JSPS).

■ REFERENCES

(1) Capadona, J. R.; Shanmuganathan, K.; Tyler, D. J.; Rowan, S. J.; Weder, C. *Science* **2008**, *319*, 1370−1374.
(2) Capadona, J. R.; Van den Berg, O.; Capadona, L. A.; Schroeter, M.; Rowan, S. J.; Tyler, D. J.; Weder, C. *Nat. Nanotechnol.* **2007**, *2*, 765−769.
(3) Juntaro, J.; Pommet, M.; Kalinka, G.; Mantalaris, A.; Shaffer, M. S. P.; Bismarck, A. *Adv. Mater.* **2008**, *20*, 3122−3126.
(4) Eichhorn, S. J. *Soft Matter* **2011**, *7*, 303−315.
(5) Uetani, K.; Yano, H. *Biomacromolecules* **2011**, *12*, 348−353.
(6) Shinoda, R.; Saito, T.; Okita, Y.; Isogai, A. *Biomacromolecules* **2012**, *13*, 842−849.
(7) Ishii, D.; Saito, T.; Isogai, A. *Biomacromolecules* **2011**, *12*, 548−550.
(8) Tatsumi, D.; Ishioka, S.; Matsumoto, T. *Nihon Reoroji Gakkaishi* **2002**, *30*, 27−32.
(9) Uetani, K.; Yano, H. *Langmuir* **2012**, *28*, 818−827.
(10) Ebeling, T.; Paillet, M.; Borsali, R.; Diat, O.; Dufresne, A.; Cavaillé, J.-Y.; Chanzy, H. *Langmuir* **1999**, *15*, 6123−6126.
(11) Bercea, M. *Macromolecules* **2000**, *33*, 6011−6016.
(12) Deegan, R. D.; Bakajin, O.; Dupont, T. F.; Huber, G.; Nagel, S. R.; Witten, T. A. *Nature (London)* **1997**, *389*, 827−829.
(13) Layani, M.; Gruchko, M.; Milo, O.; Balberg, I.; Azulay, D.; Magdassi, S. *ACS Nano* **2009**, *3*, 3537−3542.
(14) Ming, T.; Kou, X.; Chen, H.; Wang, T.; Tam, H.-L.; Cheah, K.-W.; Chen, J.-Y.; Wang, J. *Angew. Chem.* **2008**, *120*, 9831−9836.
(15) Sharma, R.; Lee, C. Y.; Choi, J. H.; Chen, K.; Strano, M. S. *Nano Lett.* **2007**, *7*, 2693−2700.
(16) Israelachvili, J. N. *Intermolecular and Surface Forces*, 2nd ed.; Academic Press: London, 1992.
(17) Doi, M.; Edwards, S. F. *The Theory of Polymer Dynamics*; Oxford University Press: New York, 1986.
(18) Wise, L. E.; Murphy, M.; D'Addieco, A. A. *Pap. Trade J.* **1946**, *122*, 35−43.
(19) Deegan, R. D. *Phys. Rev. E* **2000**, *61*, 475−485.
(20) Dong, X. M.; Kimura, T.; Revol, J.-F.; Gray, D. G. *Langmuir* **1996**, *12*, 2076−2082.
(21) Pan, J.; Hamad, W.; Straus, S. K. *Macromolecules* **2010**, *43*, 3851−3858.
(22) Onsager, L. *Ann. N.Y. Acad. Sci.* **1949**, *51*, 627−659.
(23) Martín, Á. G.; Gelderblom, H.; Lohse, D.; Snoeijer, J. H. *Phys. Rev. Lett.* **2011**, *107*, 085502.